A Fluorescent Polymer for Facile One-Step Writing of Polychromic Hidden Information in Flexible Films

Xiaoyuan Liu, Moritz E. Kleybolte, Mhamad Hantro, Cole Butler, Sergey I. Vagin, Colin van Dyck, Michael Fleischauer, Jonathan G. C. Veinot, Bernhard Rieger, and Alkiviathes Meldrum*

A poly(para)phenylene conjugated polymer is developed to store information via a quick and facile optical writing method. After exposure to UV light, co-fluorescence (films with two or more written emission colors –, i.e., "double-on") and "on-off" states are written into the flexible polymer films. The hidden information is invisible under ambient lighting and can only be read with an appropriate light source, optical filter, and/or magnifier, thus providing a level of security for information encoded into the films. The physical and chemical mechanisms are discussed responsible for the rapid fluorescence changes that occur under UV exposure and demonstrate microscale multi-colored artwork and hidden QR codes written into pliable and freestanding films. Depending on the preparation, the written patterns remained easily visible and stable after exposure to water and to ambient levels of UV background radiation.

1. Introduction

The writing of hidden text has a rich history dating back to ancient times. One of the earliest accounts of invisible ink is attributed to Aeneas Tacticus around the 4th century BC,[1] who described methods to transmit secret messages, but he did not state the exact type of ink. Pliny the Elder may have used the juice of the Mediterranean spurge plant to scribe invisible letters nearly 2000 years ago.[2] Around the same time, Ovid described how milk could be used to write secret messages between two lovers and even suggested various places to hide such messages.[3] These ancient methods generally involved the use of plant- or animal-based "inks" that require mild heating to make the inscriptions permanently visible.

Writing hidden information for modern security or anti-counterfeiting applications demands that at least one, but ideally multiple, special viewing conditions be met in order to read the information. Two-photon fluorescent (TPF) inks are a novel possibility for writing hidden information, in which illumination with an infrared laser is used to view the otherwise invisible writing.[4] However, this advantage is also a drawback because lasers are expensive and those with sufficient power for TPF are safely operated in a laboratory setting. Polarized light devices present another modern option, in which information can be read by polarizing the incident light and/or by reading the reflected beam with an appropriately-oriented analyzer.[5] From the point of view of security printing, however, polarizing elements are so inexpensive, simple, and widely accessible that they offer a limited degree of security. Fluorescent devices represent the third main option, where in this case information visibility requires ultraviolet (UV) flashlight illumination.[6,7] This method is promising because of the ability to combine different emission colors for high-density multiplexed encoding, it requires much more modest illumination conditions compared to TPF strategies, and the necessary light source and optics can be incorporated into existing scanners without major safety concerns. The level of obfuscation can be enhanced by requiring specific optical filters to easily view the written information, as we will demonstrate using a conjugated polymer system.

Conjugated polymers (CPs) represent an important class of organic opto-electronic materials currently employed or under

X. Liu, M. Fleischauer, A. Meldrum
Department of Physics
University of Alberta
Edmonton, AB T6G 2E1, Canada
E-mail: ameldrum@ualberta.ca

M. E. Kleybolte, S. I. Vagin, B. Rieger
Wacker Chair of Macromolecular Chemistry
Technical University of Munich
Lichtenbergstraße 4, 85747 Garching bei München, Germany

M. Hantro, C. van Dyck
Department of Physics
Université de Mons
20 place du Parc, Mons 7000, Belgium

C. Butler, J. G. C. Veinot
Department of Chemistry
University of Alberta
Edmonton, AB T6G 2G2, Canada

M. Fleischauer
National Research Council – Nanotechnology Research Centre
Edmonton, AB T6G 2M9, Canada

The ORCID identification number(s) for the author(s) of this article can be found under https://doi.org/10.1002/adfm.202402033

**ADVANCED
SCIENCE NEWS**

www.advancedsciencenews.com

**ADVANCED
FUNCTIONAL
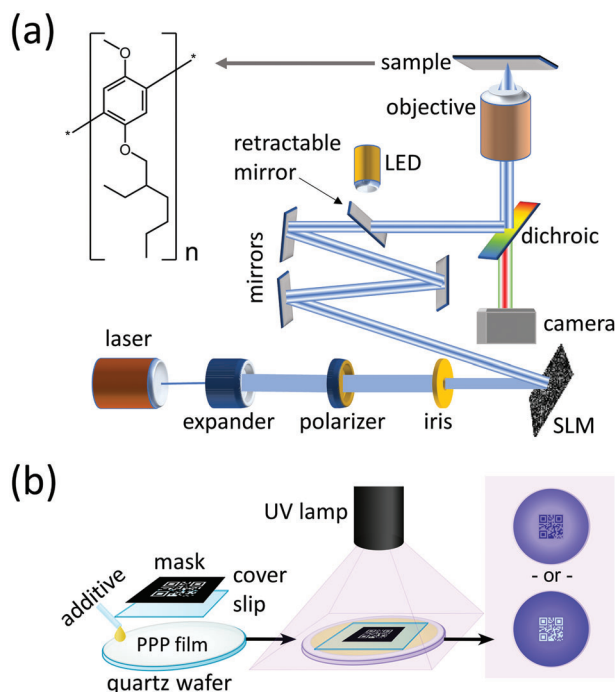MATERIALS**

www.afm-journal.de

Figure 1. Two methods for fluorescent writing on the polymer. a) Diagram of the spatial light modulator setup. The inset shows the MEH-PPP repeat unit. b) Diagram of the masked UV-exposure setup.

development for numerous applications including fluorescent biosensors,[8] organic light-emitting diodes,[9] lasers,[10] photovoltaic cells,[11] and energy storage.[12] Patterning of CP films into predefined regions has been proposed for the development of organic light-emitting displays,[13] cloaked barcodes or quick-response (QR) codes,[14] inkjet imaging and printing,[15] fluorescence sensing,[16] organic bioelectronics,[17] and the development of emissive photonic devices.[18] Several methods have been demonstrated for patterning CPs including conventional UV lithography,[19] electron beam lithography,[20] inkjet printing,[14,21] two-photon laser lithography,[13] and self-assembly.[15,22]

While a variety of chemical means can be used to derive different emission spectra from the same polymer framework or repeat unit,[9,23,24] two-color co-fluorescent writing (i.e., the local modification of one fluorescence color into another) requires that the polymer structure can be changed locally and in situ. Such changes can be obtained from localized exposure to heat,[25] force,[26] pressure,[27] light, or radiation.[20] Photochromic polymers[24,28] are especially interesting because patterning can, in principle, be achieved via lithography or direct optical writing. Patterning of fluorescent CP films has been done by locally quenching the fluorescence with an electron beam;[20] however, this method is slow and expensive and has not generated co-fluorescence or the ability to quickly write hidden information. Short-wavelength laser irradiation is another option but exposure to UV light leads mainly to bleaching[29] via various photo-oxidation and chain scission processes.[30] Previous methods used to write on polymers have focused a laser beam onto the

substrate and then physically moved either the sample[14] or the laser itself;[31] once again a slow, serial process.

The poly(para)phenylenes (PPPs) are a class of conjugated polymers based on 1,4-linked benzene subunits[32] (**Figure 1**). They share many structural and photophysical similarities with the "ladder-like" polyfluorenes (PFOs), which have become a predominant class of blue-fluorescent polymers. PPPs specifically have several attractive properties including highly controllable synthesis and ease of functionalization via the attachment of the desired side-groups.[32] Polyfluorenes are well known to suffer from photobleaching due to the evolution of ketonic and phenolate defects arising from formation of carbonyl bonds during thermal (or, presumably, photo-) oxidation.[33] Especially intriguing from the point of view of fluorescence writing, hidden information, and anti-counterfeiting applications is that the formation of aryl carbonyl units (similar to those reported after thermal treatment of PPPs)[33] can lead to dramatic changes in the luminescence spectrum of conjugated polymers like PFO.[34]

In retrospect, the ability to encode fluorescent information into PPP films via direct optical writing could have been anticipated but has never been demonstrated. In this work, we will show that poly[2-(2-ethylhexyloxy)−5-methoxy(para)phenylene (MEH-PPP) and other alkoxy-substituted PPPs offer exceptional properties for direct optical writing of flexible freestanding "on-off" or co-fluorescent "double-on" films that permit their development for applications relating to artwork, security, and anti-counterfeiting.

2. Experimental Section

2.1. Polymer Synthesis

MEH-PPP with M_w = 56 kg mol^{-1} and M_n = 30 kg mol^{-1} was synthesized using modifications of previously-published procedures.[35] In brief, 1,4-dibromo-2-((2-ethylhexyl)oxy)−5-methoxybenzene was converted to the corresponding isomeric mono-Grignard derivatives using the commercially available turbo-Grignard reagent (iPrMgCl·LiCl) in dry THF. Subsequently, 0.05 mol-% of the Ni-based catalyst Ni(IPr)(PPh$_3$)Cl$_2$ was added to the resulting solution in order to start the Kumada Catalyst Transfer Polymerization. After the completion of the polymerization (typically 5 days), the product was precipitated with methanol, washed with acetone, and dried. Other alkoxy-substituted PPPs including poly[2,5-bis(hexyloxy)-(para)phenylene (BHex-PPP)] and poly[2-(2,5,8,11-tetraoxatridecan-13-yl)oxy-5-methoxy(para)phenylene (M4EG-PPP)]were synthesized in accordance with previously published methods.[35]

2.2. Sample Preparation

For solution-based samples, the as-produced MEH-PPP was dissolved in either chloroform (CFM), chlorobenzene (CBZ), toluene (TOL), or benzene at concentrations from 0.005 to 20 mg mL^{-1}. Neat films were produced by spin coating or drop casting from these solutions. Liquid films were made by dropping ≈ 0.02 mL onto a fused silica slide and immediately placing a cover slip on top. Small air bubbles were removed by gently pressing

**ADVANCED
SCIENCE NEWS**

www.advancedsciencenews.com

**ADVANCED
FUNCTIONAL
MATERIALS**

www.afm-journal.de

the cover slip until they disappeared. Solid films were produced by drop-casting (20–30 mg Ml^{-1}) onto a glass wafer and allowing it to dry for 12 hours in air.

2.3. Optical Characterization

Photoluminescence (PL) spectroscopy was performed using the combined 351 and 364 nm lines of a UV-optimized Ar^+ ion laser as the excitation source. The PL was collected with an optical fiber, passed through a 375 nm longpass filter, and sent to an intensity- and wavelength-calibrated miniature spectrometer. Absorption was done by diluting the solutions to ≈0.05 mg mL^{-1} and measuring the absorbance (using a Thorlabs' SLS204 deuterium-tungsten lamp) relative to the blank solvent. The quantum efficiency was measured in a customized integrating sphere using a 365 nm LED with a 10-nm bandpass filter for the excitation. Fourier transform infrared spectroscopy (FTIR) was performed using Nicolet iS50 FT-IR spectrophotometer equipped with an attenuated total reflection (ATR) module. The samples were drop casted onto the ATR crystal (diamond) from tetrahydrofuran (THF) solutions and the spectra were recorded after the solvent completely evaporated.

2.4. Structural Characterization

To investigate the processes responsible for the spectral shifts under UV radiation in chlorinated solvents, CFM solutions were prepared and irradiated as described above. Then the CFM was allowed to evaporate under ambient conditions and the residue was analyzed by means of gel-permeation chromatography (GPC) in THF as an eluent (Varian GPC-50 plus, PLgel MIXED-C columns 600 mm in length, measurement against polystyrene standards) as well as by proton magnetic resonance (^1H NMR) spectroscopy in deuterated chloroform ($CDCl_3$) using a Bruker AV-Neo 400 MHz instrument.

2.5. UV Exposure

To measure the changes to the polymer under UV exposure, 1-mL glass vials of PPP solution were placed under a 4 W mercury lamp equipped with a 365 nm bandpass filter (10 nm filter width). The vials were covered with parafilm to avoid evaporation, lined up on a flat table, and irradiated for a period of 1 hour (fluence = ≈4×10^{21} photons cm^{-2}). A Sony a6400 camera mounted on a tripod took pictures every 30 seconds to track the process. Fluorescence spectra were taken as described above for the initial and final states.

2.6. Fluorescence Microscopy and Optical Writing

Fluorescence microscopy was done on a Nikon TE2000e inverted fluorescence microscope. A low-power 365 nm LED was used for routine imaging of the photosensitive polymer. For laser writing, a Skylark 349NX laser ($\lambda = 349$ nm) operated at a nominal power of 20–50 mW was used. The beam was passed through a beam expander, a polarizer, and a controllable iris, and was then incident on a Holoeye Pluto-2.1-99 spatial light modulator (SLM; Figure 1a). A PC was used to send Fourier phase holograms of the desired images to the SLM. The resulting spatially modulated beam was then projected into the microscope, demagnified through the objective lens, and focused onto the polymer. Both solid (spin coated) and liquid polymer films were exposed in this manner. After exposure the laser was turned off and the low-power LED was used for fluorescence imaging.

Other films were exposed through a photomask with a broadband UV light source (Figure 1b). The photomasks were prepared by printing onto a transparency paper with a standard commercial laser printer. Exposures were done using an irradiance of 60 mW cm^{-2} for up to 60 minutes. Freestanding MEH-PPP films were prepared by drop casting a 15 mg mL^{-1} solution in benzene on a quartz wafer and allowing it to dry overnight. Photomasked UV exposure was performed on the following day and the films were then removed from the wafer by gently detaching them with a pair of plastic tweezers. In some cases, a benzoyl chloride (BzCl) liquid film was added by dropping BzCl directly on a dry polymer film and placing a cover slip on top.

2.7. Density Functional Theory

Quantum chemistry calculations were carried out using the Gaussian 16 software platform.[36] Infrared (IR) spectra were calculated using the semi-local BP86 DFT functional[37] and the 6–31g(d,p) basis set. This functional was chosen for its close-to-unity rescaling factors (see Supporting Information) for harmonic frequencies.[38] Excited state geometries, frequencies and oscillator strengths were computed using TD-DFT, at the CAM-B3LYP level of theory,[39] also using the 6–31g(d,p) basis set. Here calculations were reported on finite oligomers made of up to nine repeated units. For most excited state calculations, a 5-mer was used unless specified otherwise. The chain length dependence of the IR and emission properties was minimal (see the Supporting Information); therefore, a shorter and finite oligomer can model the polymer structure. Moreover, to reduce the computational complexity, the long alkyl side chains were limited in methyl groups. This was justified in the supporting information, in which it was shown that the side chains do not play any role in the fluorescence properties of the polymer. Different solvent conditions were considered using the CPCM implicit solvation model[40] in the calculations for two solvents (CFM and TOL). In the calculations that the solvent, as a dielectric medium, does not play a significant role in the IR or the UV/VIS properties were observed.

3. Results and Discussion

3.1. Properties and Mechanisms

As synthesized, the MEH-PPP has a molecular weight of M_n = 30–120 kg mol^{-1} (M_w = 56–376 kg mol^{-1}) depending on the synthesis parameters used. It appears as a dry whitish powder soluble in organic solvents of moderate-to-low polarity such as TOL, tetrahydrofuran (THF), CBZ, benzene, or CFM. It has a
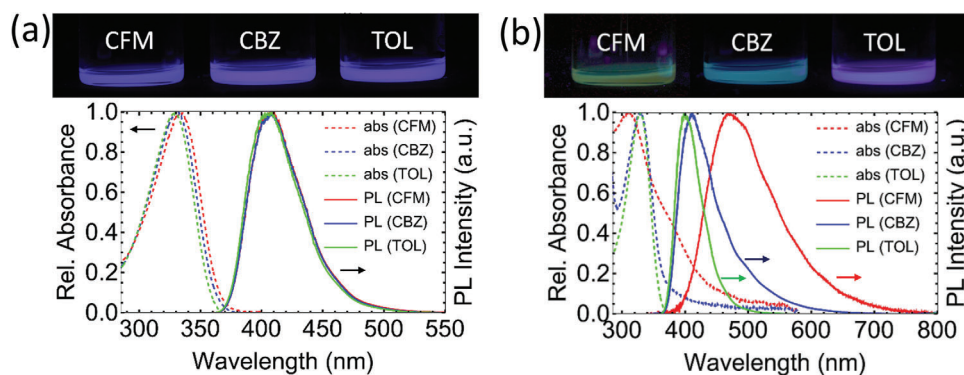
**ADVANCED
SCIENCE NEWS**

www.advancedsciencenews.com

**ADVANCED
FUNCTIONAL
MATERIALS**

www.afm-journal.de

Figure 2. a) Normalized absorbance and photoluminescence spectra of 0.5 mg mL^{-1} MEH-PPP in chloroform (CFM), chlorobenzene (CBZ), and toluene (TOL). A photograph of the solutions taken under a blacklight is shown across the top of each graph, showing the strong violet fluorescence; b) Normalized absorbance and photoluminescence spectra for the same samples after exposure to a 365 nm broadband lamp to a fluence of ≈4 × 10^{21} photons/cm^2 incident from the top of the vials. Exposure and contrast were slightly adjusted for clear viewing. Un-adjusted images are shown in Figure S1 (Supporting Information).

strong violet fluorescence in solution with an emission maximum at ≈405 nm (**Figure 2a**), while the maximum absorbance appears at ≈330 nm. The fluorescence quantum efficiency was measured to be 33%, 53%, and 34% in chloroform, chlorobenzene, and toluene, respectively, with a repeat error of around 5%. The higher efficiency in CBZ compared to the other solvents could arise from the viscosity, which is ≈ 50% higher for CBZ than for the other two solvents. A film spin coated from THF had a quantum efficiency of 60% and the as-prepared raw powder gave a value of 76%, although scattering may affect the latter result. Unusually, solid MEH-PPP has a higher QE than does the dissolved form, which is useful in relation to light emission and fluorescence writing applications.

The solutions were exposed to a broadband UV lamp (λ_{ex} = 365, full width at half maximum of 10 nm) with an incident power of 1.5 W for a period of 60 minutes (Figure 2b). Whereas in TOL the fluorescence remained nearly unchanged, in CBZ a long-wavelength tail developed and the emission changed from violet to blue (Figure 2). In CFM, the PL changed more dramatically, peaking at 470 nm and extending well into the region past 700 nm, appearing as a pale green to the eye after an exposure to ≈4 × 10^{21} photons cm^{-2} at a wavelength of 365 nm. After irradiation, the quantum efficiency of the irradiated solutions was 1%, 12%, and 29% in CFM, CBZ, and TOL, respectively. The color-changing processes occurred much more slowly for irradiation at 400 nm, which lies just outside the absorption band of the polymer.

Several methods were used to evaluate the photochemical processes leading to the fluorescence shift of MEH-PPP. GPC analysis revealed a decrease of M_n from 30 kg mol^{-1} to 8 kg mol^{-1} for MEH-PPP irradiated in CFM and an increase in the dispersity from 1.85 to 3.00, consistent with random chain scission.[35,41] All the ^{1}H NMR signals in the irradiated MEH-PPP were slightly broadened and new shoulders appeared at lower chemical shift side of the peaks assigned to aromatic protons as well as to the aliphatic protons closest to the oxygen atoms (Figure S2, Supporting Information). These could originate from the new end-groups of the polymer chains after scission. At the same time, new infrared absorption bands developed in the range of ≈1730–1710 (band I), 1676–1650 (band II), and 1612–1579 cm^{-1} (band

III; Figure S3, Supporting Information). Bands I and III developed in all irradiated samples and correlated with a decrease in the overall emission intensity. In contrast, Band II, which is in the range typically observed for aryl carbonyl defects,[33,34] only developed when the polymer was exposed either in chloroform or in toluene with added BzCl (an acyl chloride), and it was connected with the strong fluorescence redshift. Chloroform produces phosgene upon UV-irradiation when traces of oxygen are present, and thus the photochemical properties were likely associated with strong acylating agents (phosgene or BzCl).

For a PPP film with a thin liquid layer of BzCl dropped on top, the fluorescence of MEH-PPP was initially completely quenched. However, it was rapidly activated under UV irradiation, converging to a strongly red-shifted spectrum broadly but not exactly similar to that observed after exposure in CFM (**Figure 3**). While the PPPs were good electron donors,[32] BzCl has long been known for its electron-accepting character[42] and is likely to receive an electron from the excited state of MEH-PPP, quenching the emission. However, there must be a parallel photochemical reaction between MEH-PPP and BzCl that generates emissive defect states not too different from those formed in chloroform (i.e., **Figure 4c,d**) which were not so electron rich and become emissive even in the presence of excess BzCl. Thus, the "native" MEH-PPP fluorescence is initially quenched (see Figure 3), but as the emissive defects, perhaps similar to that shown in Figure 4e, form under UV exposure, the corresponding red-shifted fluorescence will increase from the initially dark state. This process enables the turn-on optical writing of the emissive states without the original violet co-fluorescence observed in films cast from other solvents.

DFT calculations showed that the ground state of the pristine MEH-PPP is characterized by a 52° twist angle between the phenyl rings (Figure 4a; Figure S4, Supporting Information) and a strong fluorescence peak (oscillator strength about 1.9) at 403 nm in good agreement with PL measurements. Band I originates from the oxidation of the side chains in the pristine structure, with conversion of phenyl alkyl ether moieties into phenyl ester groups (Figure S5, Supporting Information). This localization on the side chains explains why Band I is unrelated to the fluorescence redshifts. An absorption at ≈1612 cm^{-1} (Band III)

**ADVANCED
SCIENCE NEWS**

www.advancedsciencenews.com

**ADVANCED
FUNCTIONAL
MATERIALS**
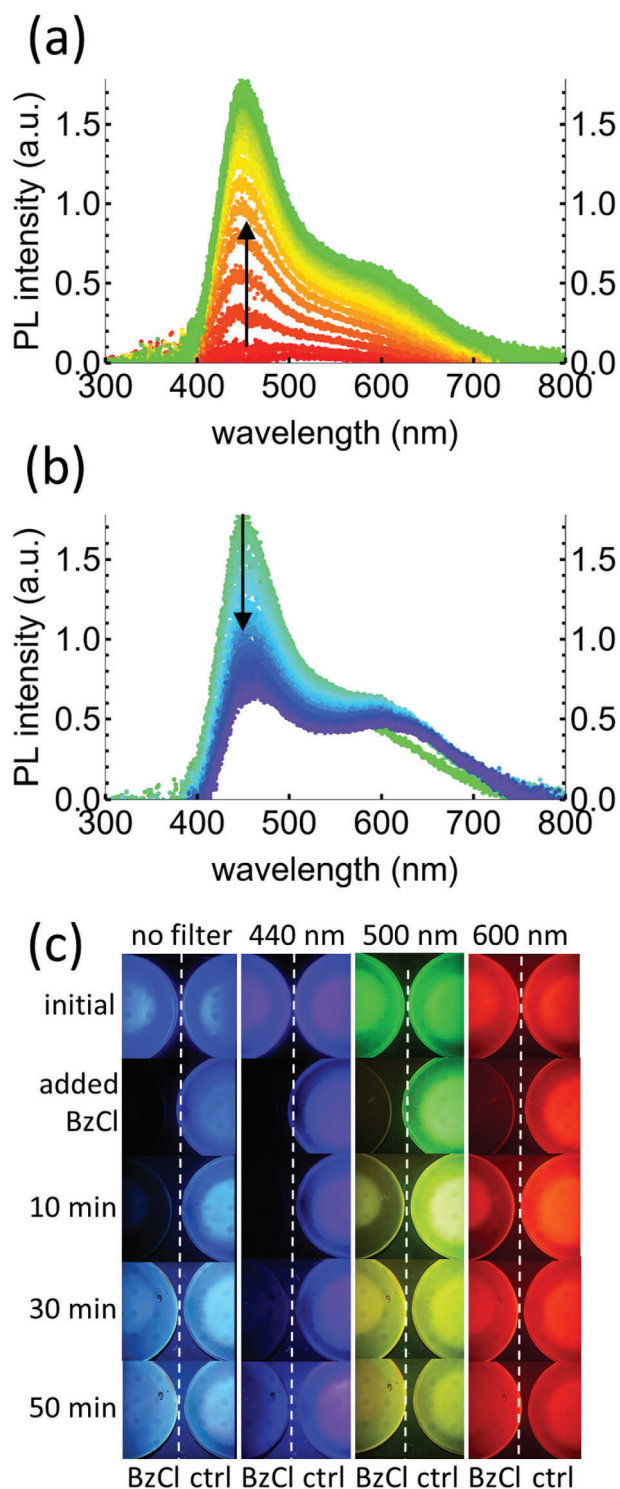
www.afm-journal.de

Figure 3. a) PL spectra of MEH-PPP in benzoyl chloride. The colors from red to green are for the first 20 minutes of UV laser exposure during which the PL increased in intensity; b) The same as in (a) showing the subsequent decrease in intensity from 20 to 180 minutes. c) MEH-PPP spin-coated films after placing several drops of BzCl and then exposing them with a 365 nm broadband lamp for 10, 30, and 50 minutes. Images were taken with no filters, a 440 nm bandpass filter, and with 500 and 600 nm long pass (LP) filters. The left image on each color strip shows a sample with BzCl added, and the right-side images are for a film exposed without BzCl.

is theoretically predicted for ketonic C = O double bonds along the conjugated chain (Figure 4b; Figure S6, Supporting Information). This defect acts as an acceptor for charge transfer excitations from the neighboring pristine repeat units and leads to an emission peak (oscillator strength about 0.07) computed at ≈667 nm. These two IR absorption bands occurred in all irradiated samples; whereas only those irradiated in the presence of CFM or BzCl developed the extra maxima between 1650–1676 cm^{-1} (Band II). Therefore, it can be presumed that those defects which produce IR-peaks in Band II may be partly responsible for the pronounced fluorescence redshift when MEH-PPP is activated by UV light in the presence of strong acylating agents.

DFT indicated the main defects responsible for Band II. First, we find that the "keto-fused bis-quinone" defect (Figure 4c) promotes a 1676 cm^{-1} IR band with a low-oscillator-strength (≈0.01) fluorescence calculated at 1125 nm. Meanwhile, a second "fluorenone-like" defect (Figure 4d) shows a strong IR-absorption calculated at 1650 cm^{-1}, also consistent with the experimental data for Band II. These two defects are presumed to arise from double acylation in the presence of chloroform (specifically due to its decomposition to phosgene). Interestingly, the fluorenone-like defect has a calculated emission peak at 525 nm with a high oscillator strength (0.31) associated with an excitation localized on the defect (see Figure S7, Supporting Information for an orbital representation) and it may, thus, be mainly responsible for the observed fluorescence redshift when MEH-PPP is exposed to UV light in the presence of chloroform. Another band-II defect can arise in the case of acylation in the presence of BzCl (Figure 4e). This defect has an IR band at 1655 cm^{-1}, an oscillator strength of 0.073 and an emission peak at 715 nm. It may be partly responsible for the extended red tail in samples exposed in contact with BzCl. While these various defects do not reproduce exactly the observed PL signal (for example, the strong peak just below 500 nm from films in contact with BzCl was not reproduced from DFT), an abundance of additional effects, including the extended sidechains, other possible defects, charge transfer, and intra- and inter-chain interactions affect the PL in solid polymer films.

3.2. Microscopic Optical Writing

The strong fluorescence changes induced by ultraviolet exposure permit the writing of co-fluorescent images, letters, or artwork. This can be achieved either by a fluorescence shift (as shown in Figure 2) or by activation from the dark state (as in Figure 3). For this purpose, a "tabula rasa" was first made by placing a drop of the polymer solution (50% CFM and 50% CBZ by volume) on a glass slide and putting another slide on top to form a thin liquid layer between the slides (i.e., see Figure 1b). The sample was placed on a microscope stage and illuminated with a 349-nm laser beam on which the word "BLUE" was holographically encoded with the spatial light modulator. A higher CFM concentration in the solvent leads to much faster writing, so the desired exposure time was controlled by varying the ratio of CFM to CBZ used as a mixed solvent. Mixtures with more CBZ were preferred; otherwise, while still in the liquid form the image can be overwritten in a matter of seconds by the subsequent low-intensity fluorescence imaging process itself.
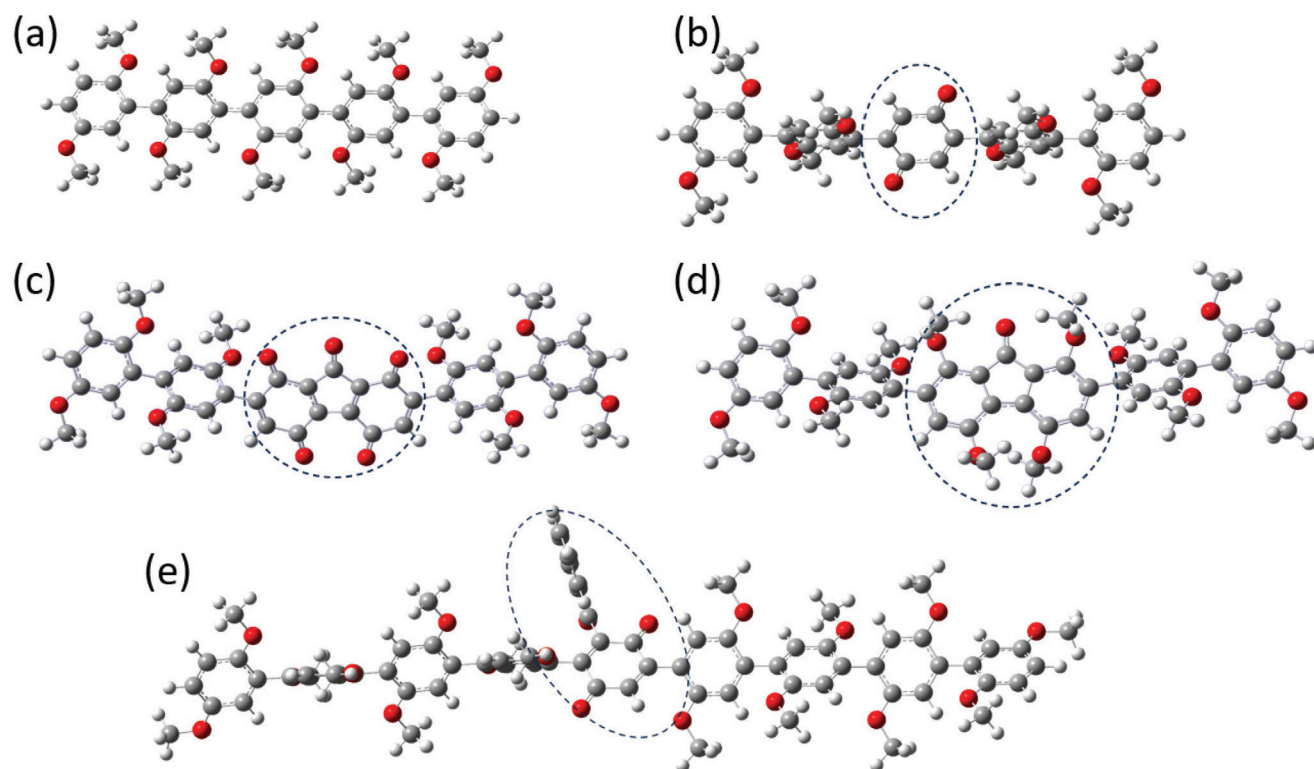
2402033 (5 of 11)

**ADVANCED
SCIENCE NEWS**

www.advancedsciencenews.com

**ADVANCED
FUNCTIONAL
MATERIALS**

www.afm-journal.de

Figure 4. Main IR-active defects in PPP. a) pristine 5-mer; b) benzoquinone-type defect (Band III); c) keto-fused bis-quinone defect (Band II); d) Band-II-type keto-fused bis-hydroquinone (fluorenone-like) defect (also); e) Band-II phenyl defect from irradiation of MEH-PPP with BzCl. The calculations were done using the shorter methyl groups on the side chains, as required for computational limits.

Upon exposure with the holographically encoded UV laser, the 256-µm-tall lettering appeared as a bluish fluorescence on a deep blue-violet background (**Figure 5a**). The background and the light speckling texture in the writing arises from the imperfect phase modulation associated with the spatial light modulator and projection optics. After ≈2 minutes the laser beam was turned off and the region was imaged with a low-intensity UV LED. The letters are just barely observable as a pale greenish fluorescence on a blue background (Figure 5b). The laser was then turned on for 15 more minutes (Figure 5c) and then the LED was again used to image the result (Figure 5d). By this point the lettering had changed to red fluorescence on a teal fluorescent background. The process was an order of magnitude faster when pure CFM was used as the solvent in the liquid film. The writing process would not occur at all, however, with solvents such as toluene or THF.

Different colors can, moreover, be written into the liquid films according to the exposure time. Shorter exposures change the originally blue fluorescence to a greenish color, and eventually a yellow or orange-red emission is obtained. By superimposing images exposed for different lengths of time, one can obtain multi-colored composite images such as the stylized apple tree shown in Figure 5k–m. The Chinese characters for green (Figure 5e,f), yellow (Figure 5g,h), and orange (Figure 5i,j) were formed by varying the exposure time to obtain greenish-yellow to orange-red fluorescence. The intensity of the blue fluorescence monotonically decreases under UV exposure, while that of the red fluorescence increases as a function of exposure time (Figure S8,

Supporting Information). The images were preserved after the liquid film fully dried via evaporation from the edges of the slides (e.g., Figure 5m).

To make solid flexible films for laser writing with the spatial light modulator, we added polyethylene sheets (PE; plain sandwich bags) between the glass slides and deposited a drop of the MEH-PPP in the same CBZ/CFM solution between the PE sheets. After exposure with the spatial light modulator, the resulting PE – MEH-PPP – PE sheet was removed and illuminated. In normal ambient lighting the written letters are invisible and the sheet is completely transparent (**Figure 6a**), but the writing was easily observable under a handheld UV flashlight. The free-standing triple-layer film was completely flexible (as shown in Figure 6, in which the sheet is bent around a 90° curve) and the written lettering was stable over a period of at least 8 weeks stored in air.

MEH-PPP can also be written directly in the solid state (i.e., without using a solvent during the exposure) by a more prolonged UV irradiation. The solid films mainly bleached by ≈ 15% before gradually stabilizing and then slowly activating the red fluorescence, while the violet emission decreased at the same time. Compared to the liquid films, the low-intensity LED had minimal effects on the solid film fluorescence. These differences can be explained by the observation that direct exposure of dry films to UV radiation leads to the less strongly emitting benzoquinone defect (Figure 4b); whereas exposure of the polymer dissolved in CFM or in contact with BzCl also produces the more strongly emissive Band-II defects (Figure 4d,e).
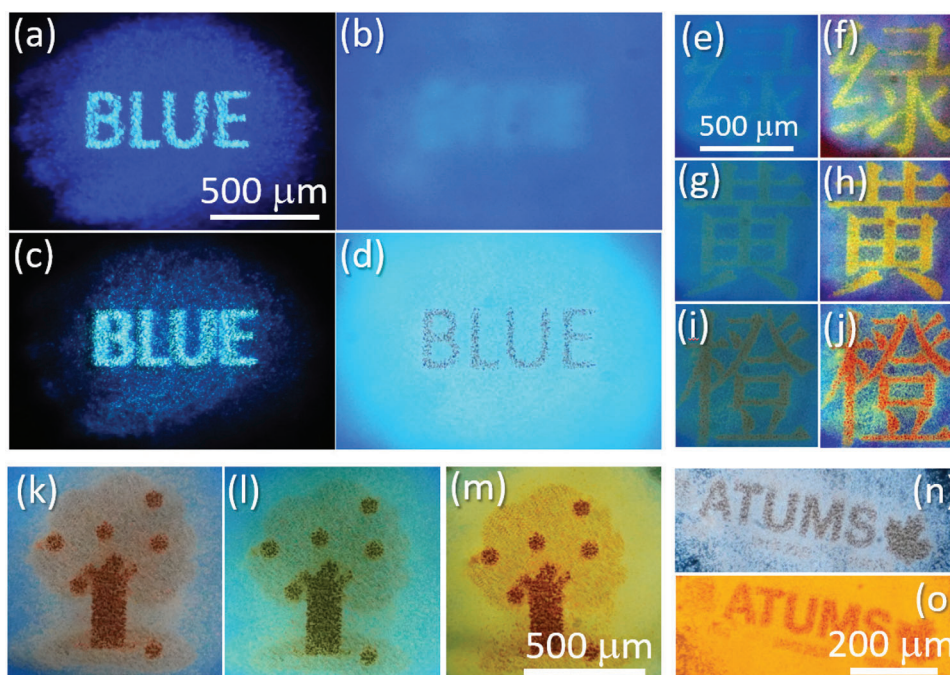
ADVANCED
SCIENCE NEWS

www.advancedsciencenews.com

ADVANCED
FUNCTIONAL
MATERIALS

www.afm-journal.de

Figure 5. Fluorescence image showing SLM laser writing in an MEH-PPP liquid film in the 50-50 mixture of CFM and CBZ. a) Initial laser exposure showing the word "BLUE" exposed onto the film. b) The same region with the laser turned off and instead illuminated by a 365-nm LED (broad exposure). c) Fluorescence image with the laser beam turned on for an additional 15 minutes. d) The laser was turned off and the sample was again illuminated with the LED, showing the lettering in red fluorescence on a teal background. No filtering was used; e,f) two-minute exposure without and with image auto-leveling, respectively; g,h) after 8 minutes; i,j) after 30 minutes. k,l) fluorescence images of an "apple tree" without and with a 400-nm longpass filter, respectively. m) same as in (l) after film solidification of the apple tree; n,o) The ATUMS logo without a filter and with a 500-nm longpass filter, respectively, produced by exposure of a MEH-PPP film drop casted from benzene.
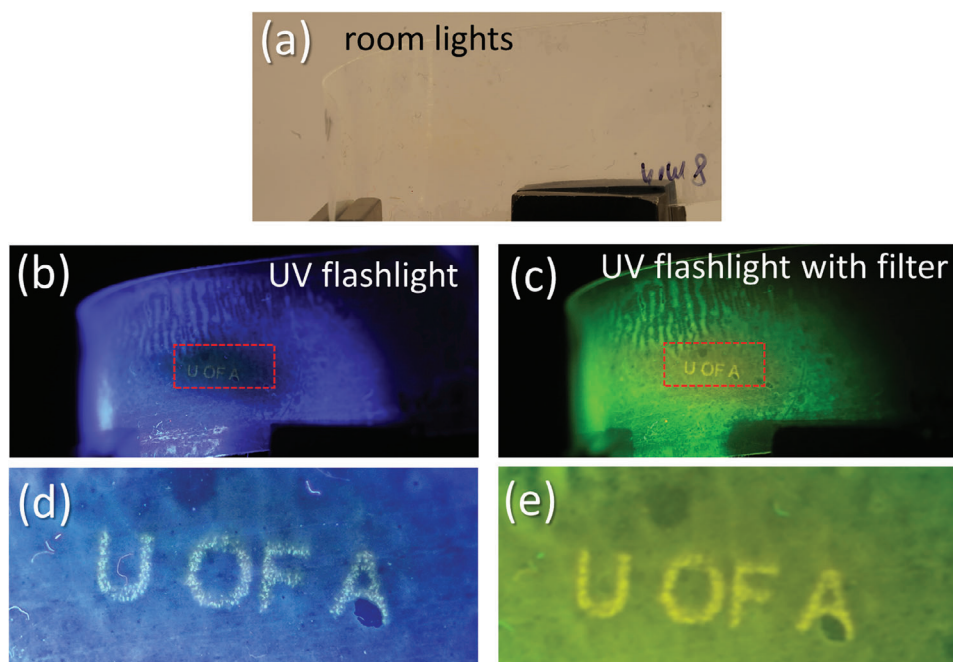

Figure 6. a) photograph of a flexible PE – MEH-PPP – PE triple-layer sheet under ambient lighting. The film is held by two clips and it is bent around a 90-degree curve; b) the same sample viewed under a UV flashlight and c) with a 500-nm longpass filter in front of the camera. d,e) Digital magnification of the lettering in (b) and (c). The flexible sample is the size of a microscope slide (≈2.5 cm x 7.5 cm).
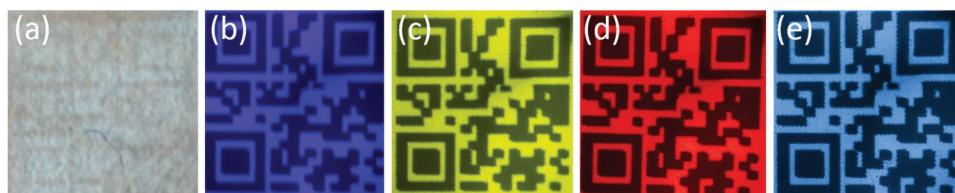
**ADVANCED
SCIENCE NEWS**

www.advancedsciencenews.com

**ADVANCED
FUNCTIONAL
MATERIALS**

www.afm-journal.de

Figure 7. A QR code written by activating the MEH-PPP film exposed while in contact with BzCl. The exposed (activated) regions of the polymer film are bright. a) a film under room lighting; b) UV illumination with a 440 nm bandpass filter in front of the camera. c) with a 500-nm longpass filter; d) with a 600-nm longpass filter; e) fluorescence image without any filtering. Scattered UV light contributes to the pale blue color in (e). The codes are 9 mm in length along each edge.

3.3. Covert QR Codes

MEH-PPP films can be used to create more than just elementary microscale artwork. Indeed, various information encoding methods can be readily applied to these films. For example, one can create hidden and color-obfuscated QR codes. Fluorescent QR codes are one of the most promising candidates for privacy-enhanced encoding or for anti-counterfeiting,[4,43] and these ideas have recently been tested for patient privacy in hospital settings.[6] Fluorescent codes using MEH-PPP can be written in parallel, which enhances the speed and lowers the cost of encoding the data. In contrast to two-photon fluorescent inks, an expensive and potentially dangerous laser is not required to read the code in everyday settings. Moreover, direct writing into flexible polymer sheets enables the production of durable and waterproof codes.

To illustrate this concept, we first wrote QR codes into a pristine MEH-PPP film using the BzCl activation process described in the experimental section. In this case the polymer fluorescence was initially quenched by BzCl and the Band II-type defect emission was activated by broadband UV exposure through a printed photomask. The resulting QR code was nearly invisible under room lighting (**Figure 7a**), but became easily observable through various optical filters when the sample was placed under a UV flashlight (Figure 7b–e). The imaged fluorescent code can be read with a QR code scanner on an Android or Apple smartphone equipped with commonly-available code readers. The ability to read the code successfully did, however, depend on the reader chosen and on the filtering. The yellow image (a 500-nm longpass filter in front of the camera) could be read by most apps we tested but only some apps could read the other colors.

The QR codes in Figure 7 become visible under UV lighting, but they do not offer any further security. This is essentially because the codes have good contrast and are well defined. Taking a different approach, one can use co-fluorescence to obfuscate the QR code so that it is difficult or impossible to scan without additional optics (i.e., optical filtering, to be known by the end user) and/or image processing. For this purpose, a QR code was written directly on a pristine MEH-PPP film drop cast from benzene such that the original violet luminescence remained present. Exposure locally shifts this luminescence into the longer-wavelength part of the spectrum, producing mainly the band III benzoquinone defect above. Under room lighting, the resulting code was completely invisible (**Figure 8a**) and we were unable to reveal it with image analysis. Under a UV lamp, it became vaguely apparent but was not readable with any QR code reader attempted on Android or Apple smartphones

(Figure 8b). With a 440 nm bandpass filter, a negative version of the code (i.e., dark in the exposed regions) appears somewhat visible (Figure 8c) but was also not readable. Positive versions of the code became apparent by using a 500 or 600 nm longpass filter in front of the camera (Figure 8d,e). Several QR code scanners were used to test the filtered codes. None of them could read the image in (c) and only one was able to successfully read (d) and (e). However, if we instead took the red code (600-nm-longpass filter), converted it to grayscale and auto-leveled it (Figure 8f), then all of the tested scanners could read the code.

The co-fluorescent films thus offer an additional layer of obfuscation. Without optical filtering, the data is not scannable. Even by separating the red, green, and blue image channels the unfiltered codes still could not be read, fundamentally because the built-in Bayer filter is too broad to spectrally isolate the encoded features with sufficient contrast for current scanners to read them. With a longpass filter placed in front of the camera, however, the codes become readable by at least one standard smartphone QR code reader. Further image processing is required for all other tested readers, but such steps could easily be done in the code reader software; indeed, the success in scanning the filtered images (i.e., images taken with a specific filter in front of the camera) will depend on the image analysis algorithm. Nevertheless, the code in Figure 7b is faintly observable by eye and might become readable with human intervention or with more advanced image manipulation processes. If necessary, however, the information can be further obfuscated by controlling the intensity of the colors via irradiation time and chemical environment. In other words, one has a competition between how hard it is to read the code (via exposure time) and the image enhancement capability of the scanner software.

In terms of durability, the written films can be removed from the acylating agent by solvent evaporation or by physically peeling them away, and then they can be attached to various objects with adhesives. The encoded fluorescent polymer strips were found to be readable at temperatures up to 150 °C. They behaved similarly when completely submerged for two hours in water as compared to air. The response to simulated ambient UV exposure was also tested under an irradiance of ≈300 W cm⁻² (roughly 10 times the UV exposure of mid-day tropical sunlight). An interesting point here is that the result depends on the process by which the pattern was written. For example, if the pattern was written directly onto a pristine MEH-PPP film (as in Figure 8), then one relies on the benzoquinone-type defect (Figure 4b), which will also be formed under ambient UV exposure. Indeed, we observe that exposure of these films somewhat degrades the pattern over a period of about 12 hours under the simulated conditions described
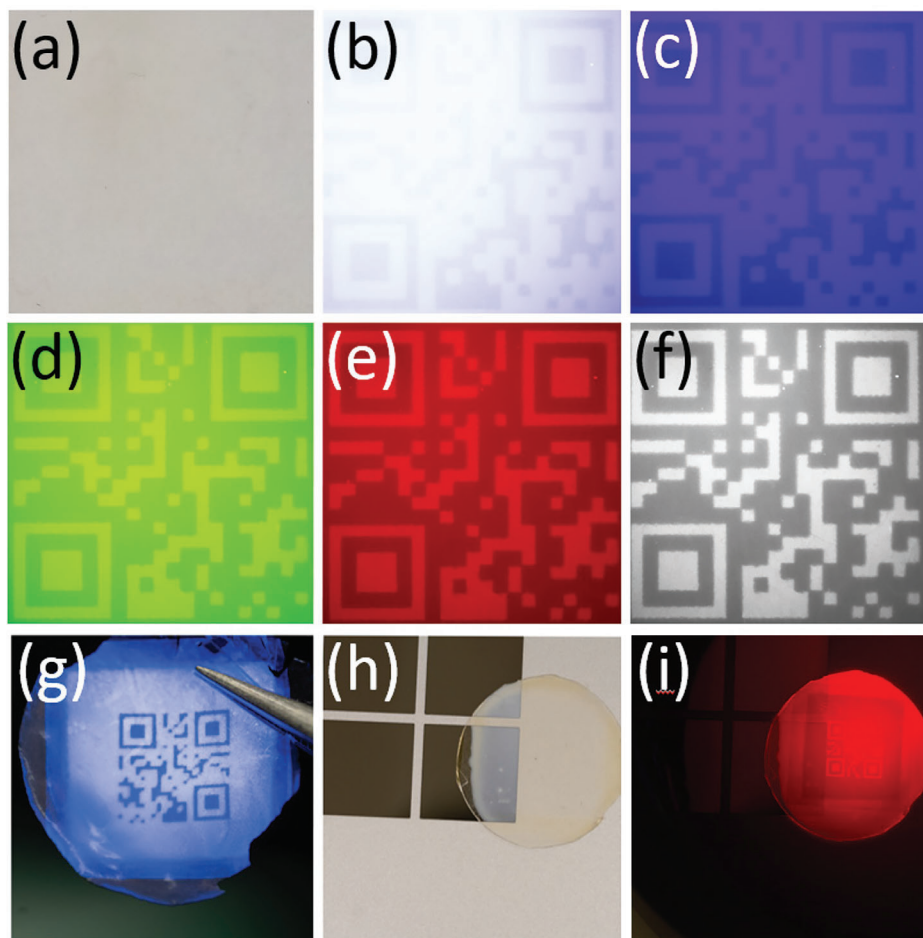
**ADVANCED
SCIENCE NEWS**

www.advancedsciencenews.com

**ADVANCED
FUNCTIONAL
MATERIALS**

www.afm-journal.de

Figure 8. a) MEH-PPP film drop cast from benzene, under room lighting. The QR code written on the film is invisible. b) Under UV lighting the code becomes barely discernable but cannot be read with a code reader. c) the sample under UV lighting with a 440-nm bandpass filter in front of the camera. The code becomes clearer but it was still not readable. The exposed regions are dark as the violet fluorescence shifts toward longer wavelengths. d) The same code using a 500 nm longpass filter. The exposed regions are bright. e) with a 600-nm longpass filter. f) After converting the red filtered image in (e) to grayscale, the resulting image became readable with most code scanners. The code measures 9 mm x 9 mm. The contrast depended on the exposure time. g) A freestanding BHex-PPP film held with a pair of tweezers under a UV flashlight. The PPP films can be affixed to a laptop PC and imaged under ambient lighting h) or with a UV lamp and a 600-nm longpass filter i).

above (300 W m^{-2} at 365 nm). On the other hand, generating the Band-II defect states (Figure 4d,e) via acylation in CFM or BzCl generates a brighter emission that cannot be duplicated by UV exposure of the dry films. Films produced by UV exposure and subsequent removal of the acylating agent remained visible after 12 hours of UV exposure (Figure S12, Supporting Information).

Obviously, there are some issues that could be improved. For example, it was rather difficult to remove the polymer from the substrate to create freestanding films. We did this by manually scraping and pulling the films from the glass substrates, which usually damaged it by stretching or wrinkling the polymer. Removal proved easier to do with BHex-PPP than MEH-PPP. Reading the image of a QR code was straightforwardly done by taking a photo of the pattern with a consumer camera (Sony a6400) equipped with a longpass filter and then scanning the image with a smartphone). However, directly reading the code with the smartphone was difficult because the patterns were quite small (≈ 9 mm) and we found it impossible to manually hold the phone,

filter, and UV flashlight steady enough to get an exposure that was directly readable by the software. Nevertheless, these issues shouldn't be especially difficult to solve. For example, standard manufacturing processes to create large freestanding films are already widely used in industry; moreover, different side groups (e.g., BHex-PPP, as stated above) and longer chain lengths were found to improve the ability to remove the films without damaging them. Finally, the hidden QR code reading in a one-step process might be easier with larger patterns and the appropriate smartphone optics and image analysis software.

We finally comment on the simplicity of the proposed writing methods, while noting that the patterns are robust and freestanding, can be easily manipulated by hand or with tweezers, can be written on a timescale of seconds in solution form to minutes in the solid form (depending on the solvent and light intensity), and can readily be affixed to objects. First, the synthesis of alkoxy-substituted PPP is straightforward and does not require any expensive or unusual chemicals. The solvents used are

**ADVANCED
SCIENCE NEWS**

www.advancedsciencenews.com

**ADVANCED
FUNCTIONAL
MATERIALS**

www.afm-journal.de

customary for any chemical lab or manufacturing process. In other words, synthesis is simple and inexpensive and can easily be scaled up. Second, the exposures are easy to do and inexpensive – all one needs is an affordable UV flashlight and access to an office laser printer with common transparency films. Moreover, other alkoxy sidegroups on the main PPP backbone tune the transparency and allow the mechanical properties to be adjusted for better performance. In our view, this combination of properties makes alkoxy-substituted PPP an excellent candidate polymer for writing hidden information or artwork in everyday environmental settings.

4. Conclusion

Writing fluorescent structures into conjugated polymers presents a method to encode and store information using a flexible, durable, and waterproof medium. Direct writing into MEH-PPP via UV optical exposure is a fast, parallel method to encode lettering or images on scales from micrometers to centimeters or larger. Writing can be done either by on-off methods, in which only the exposed region is fluorescent, or by "double-on" co-fluorescence, in which the information is written onto a fluorescent background of a different color. In the case of the on-off method, quenching likely occurs through electron transfer from the primary excited state to nearby acceptor molecules. The long wavelength emission comes from UV-induced defects that are not susceptible to energy transfer; moreover, which emissive defect is produced depends on the exposure conditions, particularly the presence or absence of an acylating agent. Thus, the violet fluorescence can either be quenched and then re-activated as a longer-wavelength emission, or directly shifted into the green, yellow, or red parts of the spectrum through one of several possible defects, to produce double-on fluorescence with the selected color depending on the exposure time.

A device as simple as a UV lamp with a laser-printed photomask can be used to write multi-colored artwork, lettering, or scannable fluorescent QR codes into MEH-PPP films. Images show good contrast and can be read by QR code readers on Android or Apple smartphones. With co-fluorescent films, current QR code readers can only read the code if an appropriate optical filter is placed in front of the camera. The contrast between the various co-fluorescent parts of the code can be reduced or enhanced depending on the net exposure time. This method adds an additional security feature to further obfuscate the information written into the films. The films are flexible, waterproof, durable, and not chemically difficult to synthesize. Moreover, polymers (as a whole) are considered by the European Chemical Agency (ECHA) as relatively non-hazardous materials that should be exempted from registration and evaluation (Titles II and VI).[44] Thus, MEH-PPP has potential for security and anti-counterfeiting applications or even for polymer-based artwork and design.

Supporting Information

Supporting Information is available from the Wiley Online Library or from the author.

Conflict of Interest

The authors declare no conflict of interest.

Data Availability Statement

The data that support the findings of this study are available from the corresponding author upon reasonable request.

[1] a) J. F. Dooley, *Cryptologia* **2016**, *40*, 107; b) W. W. Tarn, *Classical Rev.* **1927**, *41*, 227.

[2] P. t. Elder, in *The Natural History*, Harvard University Press, Cambridge **1938**.

[3] K. Macrakis, in *Prisoners, Lovers, and Spies: The Story of Invisible Ink from Herodotus to al-Qaeda*, Yale University Press, New Haven, Connecticut **2014**.

[4] a) M. You, M. Lin, S. Wang, X. Wang, G. Zhang, Y. Hong, Y. Dong, G. Jin, F. Xu, *Nanoscale* **2016**, *8*, 10096; b) J. M. Meruga, W. M. Cross, P. Stanley May, Q. Luu, G. A. Crawford, J. J. Kellar, *Nanotechnology* **2012**, *23*, 395201; c) M. Li, W. Yao, J. Liu, Q. Tian, L. Liu, J. Ding, Q. Xue, Q. Lu, W. Wu, *J. Mater. Chem. C* **2017**, *5*, 6512.

[5] a) C. Liu, A. K. Steppert, Y. Liu, P. Weis, J. Hu, C. Nie, W. C. Xu, A. J. C. Kuehne, S. Wu, *Adv. Mater.* **2023**, *35*, 2303120; b) Z. Qin, T. Wang, H. Gao, Y. Li, H. Dong, W. Hu, *Adv. Mater.* **2023**, *35*, 2301955.

[6] K. Jiang, D. Xu, Z. Liu, W. Zhao, H. Ji, J. Zhang, M. Li, T. Zheng, H. Feng, *RSC Adv.* **2019**, *9*, 37292.

[7] J. W. Leem, H. J. Jeon, Y. Ji, S. M. Park, Y. Kwak, J. Park, K. Y. Kim, S. W. Kim, Y. L. Kim, *ACS Cent. Sci.* **2022**, *8*, 513.

[8] a) C. A. Traina, R. C. Bakus 2nd, G. C. Bazan, *J. Am. Chem. Soc.* **2011**, *133*, 12600; b) M. A. Rahman, P. Kumar, D.-S. Park, Y.-B. Shim, *Sensors* **2008**, *8*, 118.

[9] L. Dai, B. Winkler, L. Dong, L. Tong, A. W. H. Mau, *Adv. Mater.* **2001**, *13*, 915.

[10] H. Xia, C. Hu, T. Chen, D. Hu, M. Zhang, K. Xie, *Polymers* **2019**, *11*, 443.

[11] a) K. Coakley, M. D. McGehee, *Chem. Mater.* **2004**, *16*, 4533; b) S. E. Shaheen, C. J. Brabec, N. S. Sariciftci, F. Padinger, T. Fromherz,

J. C. Hummelen, *Appl. Phys. Lett.* **2001**, *78*, 841; c) S. Gunes, H. Neugebauer, N. S. Sarisiftci, *Chem. Rev.* **2007**, *107*, 1324; d) A. Kim, J. K. Dash, P. Kumar, R. Patel, *ACS Appl. Electron. Mater.* **2021**, *4*, 27.

[12] J. F. Mike, J. L. Lutkenhaus, *J. Polym. Sci., Part B: Polym. Phys.* **2013**, *51*, 468.

[13] Y. Xu, F. Zhang, X. Feng, *Small* **2011**, *7*, 1338.

[14] A. Jaiswal, S. Rani, G. P. Singh, S. Saxena, S. Shukla, *JPhys Photonics* **2021**, *3*, 034021.

[15] S. Jeon, S. Park, J. Nam, Y. Kang, J. M. Kim, *ACS Appl. Mater. Interfaces* **2016**, *8*, 1813.

[16] Y. S. Jung, W. Jung, H. T. Tuller, C. A. Ross, *Nano Lett.* **2008**, *8*, 3776.

[17] S. Kee, P. Zhang, J. Travas-Sejdic, *Polym. Chem.* **2020**, *11*, 4530.

[18] M. Deutsch, Y. A. Vlasov, D. J. Norris, *Adv. Mater.* **2000**, *12*, 1176.

[19] H. Yamagishi, T. Matsui, Y. Kitayama, Y. Aikyo, L. Tong, J. Kuwabara, T. Kanbara, M. Morimoto, M. Irie, Y. Yamamoto, *Polymers* **2021**, *13*, 269.

[20] E. Fisslthaler, M. Sezen, H. Plank, A. Blümel, S. Sax, W. Grogger, E. J. W. List, *Macromol. Chem. Phys.* **2010**, *211*, 1402.

[21] B. Yoon, D. Y. Ham, O. Yarimaga, H. An, C. W. Lee, J. M. Kim, *Adv. Mater.* **2011**, *23*, 5492.

[22] M. H. Nurmawati, R. Renu, P. K. Ajikumar, S. Sindhu, F. C. Cheong, C. H. Sow, S. Valiyaveettil, *Adv. Funct. Mater.* **2006**, *16*, 2340.

[23] a) H. A. M. van Mullekom, J. A. J. M. Vekemans, E. E. Havinga, E. W. Meijer, *Mater. Sci. Eng. R Rep.* **2001**, *32*, 1; b) F. Meyers, A. J. Heeger, J. L. Brédas, *J. Chem. Phys.* **1992**, *97*, 2750; c) R. M. Walczak, J. R. Reynolds, *Adv. Mater.* **2006**, *18*, 1121; d) Z. D. Yu, Y. Lu, J. Y. Wang, J. Pei, *Chemistry* **2020**, *26*, 16194; e) M. P. Jphansson, M. Olsen, *J. Chem. Theory Comput.* **2008**, *4*, 1460.

[24] G. M. Peters, J. D. Tovar, *J. Am. Chem. Soc.* **2019**, *141*, 3146.

[25] S. Hayashi, *Mater. Adv.* **2020**, *1*, 632.

[26] T. Han, X. Wang, D. Wang, B. Z. Tang, *Top Curr. Chem.* **2021**, *379*, 7.

[27] D. J. Ahn, S. Lee, J.-M. Kim, *Adv. Funct. Mater.* **2009**, *19*, 1483.

[28] A. Szukalski, A. Korbut, E. Ortyl, *Polymer* **2020**, *192*, 122311.

[29] a) Q. Xu, F. Lv, L. Liu, S. Wang, *Macromol. Rapid Commun.* **2020**, *41*, 2000249; b) H. Duan, J. Zhang, Y. Weng, Z. Fan, L. J. Fan, *ACS Appl. Mater. Interfaces* **2022**, *14*, 32510; c) G. Kwak, M. Fujiki, T. Sakaguchi, T. Masuda, *Macromolecules* **2006**, *39*, 319; d) X. Wang, L. C. Groff, J. D. McNeill, *Langmuir* **2013**, *29*, 13925; e) M. L. Raicoski, M. G. Vivas, *J. Phys. Chem. B* **2021**, *125*, 9887; f) W. E. Lee, H. Park, G. Kwak, *Chem. Commun.* **2011**, *47*, 659; g) T. Mehreen, S. I. Vagin, V. Kumar,

X. Liu, L. Eylert, B. Rieger, A. Meldrum, *Macromol. Chem. Phys.* **2022**, *224*, 2200294; h) S. Chambon, A. Rivaton, J.-L. Gardette, M. Firon, L. Lutsen, *J. Polym. Sci., Part A: Polym. Chem.* **2007**, *45*, 317.

[30] B. Louis, S. Caubergh, P. O. Larsson, Y. Tian, I. G. Scheblykin, *Phys. Chem. Chem. Phys.* **2018**, *20*, 1829.

[31] J. Feng, J. Zhang, Z. Zheng, T. Zhou, *ACS Appl. Mater. Interfaces* **2019**, *11*, 41688.

[32] M. E. Kleybolte, S. I. Vagin, B. Rieger, *Macromol. Chem. Phys.* **2023**, *224*, 2200441.

[33] L. Romaner, G. Heimel, H. Wiesenhofer, P. S. de Freitas, U. Scherf, J.-L. Bredas, E. Zojer, E. J. W. List, *Chem. Mater.* **2004**, *16*, 4667.

[34] L. Chen, W.-C. Chen, Z. Yang, J.-H. Tan, S. Ji, H.-L. Zhang, Y. Huo, C.-S. Lee, *J. Mater. Chem. C* **2021**, *9*, 17233.

[35] M. E. Kleybolte, S. I. Vagin, B. Rieger, *Macromolecules* **2022**, *55*, 5361.

[36] M. J. Frisch, G. W. Trucks, H. B. Schlegel, G. E. Scuseria, M. A. Robb, J. R. Cheeseman, G. Scalmani, V. Barone, G. A. Petersson, H. Nakatsuji, X. Li, M. Caricato, A. V. Marenich, J. Bloino, B. G. Janesko, R. Gomperts, B. Mennucci, H. P. Hratchian, J. V. Ortiz, A. F. Izmaylov, J. L. Sonnenberg, D. W. Young, F. Ding, F. Lipparini, F. Egidi, J. Goings, B. Peng, A. Petrone, T. Henderson, D. Ranasinghe, Wallingford, CT **2016**.

[37] a) A. D. Becke, *Phys. Rev. A Gen. Phys.* **1988**, *38*, 3098; b) J. P. Perdew, *Phys. Rev. B Condens. Matter.* **1986**, *33*, 8822.

[38] M. L. Laury, M. J. Carlson, A. K. Wilson, *J. Comput. Chem.* **2012**, *33*, 2380.

[39] T. Yanai, D. P. Tew, N. C. Handy, *Chem. Phys. Lett.* **2004**, *393*, 51.

[40] a) V. Barone, M. Cossi, *J. Phys. Chem. A* **1998**, *102*, 1995; b) M. Cossi, N. Rega, G. Scalmani, V. Barone, *J. Comput. Chem.* **2003**, *24*, 669.

[41] a) P. E. Le Marec, L. Ferry, J.-C. Quantin, J.-C. Bénézet, F. Bonfils, S. Guilbert, A. Bergeret, *Polym. Degrad. Stab.* **2014**, *110*, 353; b) S. V. Canevarolo, *Polym. Degrad. Stab.* **2000**, *70*, 71.

[42] R. C. Paul, S. L. Chadha, *Spectrochim. Acta* **1966**, *22*, 615.

[43] a) H. Zhang, X. Ji, *ACS Cent. Sci.* **2022**, *8*, 507; b) W. Ren, G. Lin, C. Clarke, J. Zhou, D. Jin, *Adv. Mater.* **2020**, *32*, 1901430; c) C. Huang, B. Lucas, C. Vervaet, K. Braeckmans, S. Van Calenbergh, I. Karalic, M. Vandewoestyne, D. Deforce, J. Demeester, S. C. De Smedt, *Adv. Mater.* **2010**, *22*, 2657; d) J. F. C. B. Ramalho, L. C. F. António, S. F. H. Correia, L. S. Fu, A. S. Pinho, C. D. S. Brites, L. D. Carlos, P. S. André, R. A. S. Ferreira, *Opt. Laser Technol.* **2018**, *101*, 304.

[44] REGULATION (EC) No 1907/2006 OF THE EUROPEAN PARLIAMENT AND OF THE COUNCIL of 18 December 2006, Official Journal of the European Union, L 396.

2402033 (11 of 11)